Modelling tidal current turbine wakes using a coupled RANS-BEMT approach as a tool for analysing power capture of arrays of turbines

Stephen R. Turnock[a], Alexander B. Phillips[a], Joe Banks[a], Rachel Nicholls-Lee[a]

[a]Fluid Structure Interactions Research Group, School of Engineering Sciences

University of Southampton, Southampton SO17 1BJ. U.K.

{srt@soton.ac.uk; abp@soton.ac.uk; jb105@soton.ac.uk;rnl@soton.ac.uk}

Corresponding Author: S.R.Turnock, Tel N: +44 2380 592488

Abstract

An improved method is developed to couple an inner domain solution of the blade element momentum theory with an outer domain solution of the Reynolds averaged Navier Stokes equations for evaluating performance of tidal current turbines. A mesh sensitivity study shows that a mesh of at least 6M cells with at least 40% of these within the turbine wake is required to ensure satisfactory convergence of the velocity deficit. In addition to the usually applied axial momentum source terms, angular momentum and turbulence intensity source terms are shown to be required to model the near wake evolution. Three different lateral turbine spacing of 2, 4 and 6 turbine diameters are used to demonstrate the influence of the effective channel blockage on the velocity distribution in the turbine bypass region, the rate of spread of the wake and the recovery of velocity distribution. A final study shows that for a fixed number of turbines minimising the lateral spacing within each row, with a small number of staggered rows spaced as longitudinally as far apart as practical, is the most effective strategy for energy capture.

Keywords

Tidal turbine; wake evolution; Computational Fluid Dynamics; tidal array energy capture; Blade Element Momentum.

1. Introduction

The tidal flow of sea water induced by planetary motion is a potential source of renewable energy if suitable systems can be designed and operated in a cost-effective manner. The interest in the development of tidal current energy converters (TEC) is evident in the schemes now proposed. Nielsen *et al* (2009) identified publicised TEC project proposals worldwide which if a typical site capacity factor of 0.3 is assumed corresponds to 5-9.7 Twh per year of electricity generation. The projected timescales for most of these projects was stated to be 5 to 10 years. Hardisty (2009) identified 253 sites worldwide in which he examined the behaviour of a single 1MW rated small array of ten 100kW turbines at each site. Even for such a relatively small installation, 0.142 Twh per year of viable electricity generation worldwide was identified.

The limited depth of most sites with sufficient energy density to allow cost-effective tidal power generation results in the need to install spatially distributed arrays of devices. This is not the case for wind turbines where there is more energy available at greater heights and it is structural constraints that limit power, Nielsen *et al* (2009). As tidal current sites have predominantly bi-directional flow, the obvious approach is to place devices close together in a line perpendicular to the flow. Physical constraints, such as the width of channels, shipping lanes or insufficient water depth will often make it impossible to site enough turbines in a single line. Consequently multiple lines across the flow are likely to be required, in the form of an array similar to those used for multi-directional wind farms. By placing multiple turbines behind one another the inflow conditions into the downstream turbines will be dependent on the wake and blockage effects of the upstream row of turbines. The ability to propose a viable tidal energy array scheme relies on an accurate assessment of the tidal resource at a specific location, Hardisty (2009). Detailed knowledge of how the local flow regime varies with depth and over short time scales comparable to the blade rate of rotation is required for the specification of the blade strength and fatigue characteristics as well as the loading imposed on the support structure,

McCann (2007). The interaction of an upstream turbine wake with a downstream turbine will make an important contribution to the unsteady fluctuations in velocity as well as to the overall kinetic energy available.

Blanchfield *et al* (2007) used a two-dimensional finite element model with turbines simulated in certain regions by increasing drag within Masset Sound in Canada, and achieved good comparisons with the analytical estimates of Garrett and Cummins (2005). Garrett and Cummins (2008) discussed the limits to power capture in channels and showed that a small number of larger devices may be the most effective strategy. They propose the approximate formula for the maximum available power P in a channel as

$$P = 0.22\rho g a Q_{\max} \qquad (1),$$

where ρ is the density, g acceleration due to gravity, a the amplitude of tidal wave and Q_{max} the maximum flow rate in the absence of energy extraction devices. Garrett and Cummins (2007) examined the interaction between multiple devices across a channel and showed that the (Lanchester-)Betz limit (C_p=16/27) for maximum efficiency of a turbine in an infinite domain is increased by a factor of $\left(1 - A/A_c\right)^{-2}$ in a channel where A is the device area and A_c the channel cross sectional area. This is equivalent to the blockage correction that should be applied to tidal energy turbines tested within a finite width channel (e.g. towing tank/cavitation tunnel), Bahaj *et al* (2007a).

Computational Fluid Dynamics (CFD), mainly Reynolds Averaged Navier Stokes (RANS) methods, has been used to provide insight into the development of the wake structure downstream of a device and can include effects of local bathymetry. Examples of such work are that of Bahaj *et al* (2007b) and Sun *et al.* (2008), who represent the influence of turbine as a specified axial momentum source associated with the thrust on the turbine. Similarly, Grant and Stallard (2008) examined how the Synthetic Eddy Model of Jarrin *et al* (2006) changes the unsteady tidal turbine wake development Antehaume *et al* (2008) considered the efficiency of Vertical Axis Tidal

Turbines (VATT) in isolation and when located in an array. They coupled a CFD code with an inner domain that represents the effect of a VATT through use of momentum sources based on blade element analysis within a cylindrical domain. It is also possible to use CFD to study the time accurate behaviour of a tidal turbine, see O'Doherty *et al* (2009), however, the computational cost will increases rapidly if a mesh insensitive solution is required. Turnock *et al* (2006) showed that for the comparable problem of evaluating ship propeller performance both a high quality and high density wake mesh as well as fine resolution of the tip vortex are required.

Experimental validation of such tidal turbine wake evolution predictions are limited, typically based on small scale experimental studies, such as Bahaj *et al* (2007b) who used porous discs in a flume and Myers and Bahaj (2007) who used a 0.4 m diameter Horizontal Axis Tidal Turbine (HATT) in a circulating water channel. Jo *et al* (2007) used a circulating water channel with twin small propellers as proxies for turbines placing them at different transverse, longitudinal and diagonal spacing and measured their free spinning RPM as a way of assessing the wake interaction. Myers *et al* (2008) examined the effect of the proximity to the seabed and free surface in a tilting flume, on the wake of a porous disk and showed some agreement compared with normalized kinetic energy evaluated using a wind turbine eddy viscosity model.

Detailed numerical predictions have been carried out for wind turbine wake evolution, see for example Sørensen and Shen (2002) and Jimenez *et al* (2008) who applied Large Eddy Simulation (LES) and applied an axial momentum source to represent the influence of the turbine disk. These methods have been compared with some degree of success with various empirical full scale measurements of wake behaviour.

The aim of the method developed in this work is to provide a sufficiently detailed representation of a single tidal turbine and its wake, yet at a computational cost that makes the assessment of multiple turbine interactions possible. The approach adopted is similar to that applied in turbomachinery to capture rotor-stator interaction where a time averaged 'frozen' wake

is applied, Sinha *et al* (2000). In particular, the influence of mesh resolution, the effect of mechanical sources of turbulence, and angular momentum induced swirl on the rate of growth of the wake and recovery of the wake velocity deficit are considered. An improved method of coupling a RANS simulation of the surrounding outer domain with a full Blade Element Momentum theory (BEMT) is applied to evaluate the actual axial and tangential momentum terms seen at the turbine location. This technique was initially developed to ensure a rapid but accurate evaluation of ship self-propulsion, Turnock *et al* (2008), Phillips *et al* (2009). It is worth noting the similarities of propeller performance prediction in the wake from a ship hull or a ship rudder in the race of a propeller, Phillips et al (2010) to that of a downstream turbine in the wake of another HATT. In both these cases the dominant influence on device performance is the circumferential averaged mean axial and tangential velocity components at a given radius rather than rapid fluctuations associated with passage of a propeller tip or hull bilge vortex, or other smaller scale turbulent features.

As an example of the use of the coupled BEMT-CFD technique the wake structure downstream of a single turbine is used to estimate the power extraction potential from a $1km^2$ array of tidal turbines.

2. Numerical Simulation of HATT Wake Development

2.1 Blade Element Momentum Theory- Inner domain

The Blade Element Momentum Theory (BEMT) code used was Cwind, developed by Barnsley and Wellicome (1993) to capture passive stall behaviour of wind turbines and modified for a tidal turbine Turnock (2006), and similarly by Batten *et al* (2008). BEMT balances the changes in fluid axial and angular momentum with velocity induction factors a_f, a' respectively, for flow through a

discrete number of annuli, typically between 10 and 20, and the work done on the corresponding blade sections at the effective local sectional angle of attack α. All the velocity components are illustrated in the blade element diagram in Figure 1 along with the resultant forces.

[insert Figure 1]

At each section the positive driving torque requires the elemental force $L\sin\varphi > D\cos\phi$ with resultant axial thrust, *T*, on the structure of $T = L\cos\phi + D\sin\phi$. The analysis uses the spanwise distribution of blade chord, *c,* and pitch, θ_t, and the two-dimensional sectional performance lift, $L = C_l(\alpha)\tfrac{1}{2}\rho V^2 c$, and drag, $D = C_d(\alpha)\tfrac{1}{2}\rho V^2 c$, of the chosen blade sections for a wide range of angles of attack, where the resultant velocity $V = \sqrt{U_w^2(1-a)^2 + r^2\Omega^2(1+a')^2}$. As the downstream turbines will be acting in a non uniform wake field the BEMT code was modified to allow for a radial variation in axial velocity based on a nominal wake fraction, $w_f = \frac{1}{2\pi}\int_0^{2\pi}(U/U_o)d\vartheta$ where $w_f = 1$ is for an undisturbed flow or otherwise calculated as the circumferential mean at a given radius *r* of the local axial flow speed U and hence $U_w = w_f U_o$. A modified Goldstein tip loss correction method accounts for the use of a finite number of blades. The code output provides power, thrust and torque at each annuli for a specified turbine diameter, D, and rate of rotation, $\Omega = 2\pi n$, to give the non-dimensional power and thrust coefficients for an annulus of area, $2\pi r\delta r$, $\delta C_p = Power/(\tfrac{1}{2}\rho U_o^3 \tfrac{\pi}{4}D^2)$ $\delta C_T = Thrust/(\tfrac{1}{2}\rho U_o^2 \tfrac{\pi}{4}D^2)$, in terms of the free stream velocity, U_o.

2.1.1 Isolated HATT BEMT analysis

The blade pitch and chord distributions of a three bladed HATT of Bahaj *et al* (2007) were used. This turbine has a 15% hub to diameter ratio. Figure 2 compares the BEMT performance prediction with the experimental data from a towing tank in terms of tip speed ratio TSR, $\lambda = \pi nD/V_\infty$, and good correlation is observed. The main differences are due to the use of a single set of sectional lift and drag data in this implementation of the BEMT.

[insert Figure 2]

2.2 RANS Implementation – Outer Domain

The outer domain motion of the fluid is modelled using the incompressible (2), isothermal Reynolds Averaged Navier Stokes (RANS) equations (3) in order to determine the mean Cartesian flow field U_i and turbulent components u_j and pressure (p) of an incompressible fluid of density ρ and kinematic viscosity ν and momentum source terms f.

$$\frac{\partial \overline{U_i}}{\partial x_i} = 0 \tag{2}$$

$$\frac{\partial \overline{U_i}}{\partial t} + \frac{\partial \overline{U_i U_j}}{\partial x_j} = -\frac{1}{\rho}\frac{\partial \overline{P}}{\partial x_i} + \frac{\partial}{\partial x_j}\left\{\nu\left(\frac{\partial \overline{U_i}}{\partial x_j} + \frac{\partial \overline{U_j}}{\partial x_i}\right)\right\} - \frac{\partial \overline{u_i' u_j'}}{\partial x_j} + f_i \tag{3}$$

The RANS equations are implemented in a commercial CFD code, ANSYS CFX(2006). The governing equations are discretised using the finite volume method. The present model uses the high-resolution advection scheme which varies between second and first order depending on spatial gradient, described in Turnock *et al* (2009), and based on a similar approach to that of Barth and Jesperson (1989). The model uses collocated (non-staggered) grids for all transport equations, and pressure velocity coupling is achieved using an interpolation scheme. The Reynolds stress tensor $-\frac{\partial \overline{u_i' u_j'}}{\partial x_j}$ in (3) is modelled using the standard k-ε model, where the

Reynolds shear stresses are calculated from the product of an isotropic eddy viscosity, ν_T, and the local rate of strain. The eddy viscosity is given by:

$$\upsilon_T = C_\mu \frac{k^2}{\varepsilon} \tag{4}$$

where k is the turbulent kinetic energy, ε is the dissipation of turbulent kinetic energy and C_μ is a constant.

2.3 Coupled RANS-BEMT Simulation

Within the RANS simulation the tidal device is modelled as a cylindrical inner domain with a diameter equal to that of the turbine and an axial length equal to 0.2D. Figure 3 illustrates the radial variation in thrust and torque acting on a turbine blade.

In order to match the BEMT calculations the turbine is divided into ten cylindrical sub-domains corresponding to ten radial slices (dr) along the blade. For each annulus the local thrust and power coefficients (δC_T and δC_p respectively) are determined by the BEMT code. The key aspect of the method applied in this case is that the upstream flow modification is already included within the BEMT (e.g. axial and tangential induction factors, a_f and a', are calculated directly). This reduces the need to run the code in an iterative fashion to ensure the correct balance of operating conditions on the turbine and within the outer domain. The RANS axial momentum source term is determined from:

$$fb_x = \frac{T}{V} = \frac{1/2\rho U_0^2 A \delta C_T}{AL} = \frac{1/2\rho U_0^2 \delta C_T}{L} \tag{5}$$

where V is the volume of the sub-domain in m^3, A is the inlet area of the sub-domain, and L is the longitudinal length of the sub-domain. The tangential source terms used to represent the swirl imparted to the flow due to the action of the turbine are similarly calculated from δC_P:

$$fb_\theta = \frac{Q}{rV} = \frac{1/2\rho U_0^3 A \delta C_P}{r\Omega AL} = \frac{1/2\rho U_0^3 \delta C_P}{r\Omega L} \tag{6}$$

where Q is the torque. The influence of these additional momentum terms in the outer domain is to provide the axial retardation of speed through the turbine. It is possible to use the approach in an iterative manner by examining the change in velocity as calculated by BEMT with that found in the CFD after the appropriate momentum terms have been included. In this case, even for the closest tangential spacing, this was not found necessary.

Figure 4 compares the axial flow factors calculated directly from the BEMT code with those realised in the RANS-BEMT simulation after convergence. The form of the curve is well represented in the RANS-BEMT simulation and gives confidence that there is no further need to iterate the process in this case, noting that it is the axial momentum loss that drives the evolution of the wake. Discrepancies arise due to the numerical implementation which applies discrete values of the required momentum source term over each of the ten annuli. This is instead of applying a continuous distribution and results from applying the momentum source terms over a finite thickness. The total thrust and torque acting on the turbine are well represented with the resulting values from the RANS-BEMT simulation matching the BEMT code to within 3%.

[insert Figure 4]

2.4.1 Influence of Turbulence Intensity

Extracting energy from the flow creates a region, known as the wake, with reduced velocity behind the turbine. Turbulent mixing in the shear layer between the freestream and wake transfers momentum back into the wake. The turbulent mixing from the radial velocity gradients behind the turbine propagates both outwards and towards the centreline of the wake, which broadens in response whilst the overall velocity deficit is reduced. This continues far downstream where the velocity deficit eventually becomes zero. The rate of wake growth depends on the turbulence intensity in the wake, I_w. The turbulence intensity downstream of the turbine is a combination of the ambient turbulence intensity, I_a, the mechanical turbulence intensity, I_m, and the wake edge shear generated turbulence Intensity, I_s, Burton et al(2001).

$$I_w = I_a + I_m + I_s \tag{7}$$

The applied turbulence closure model, in this case the standard k-ε turbulence model, given a sufficient wake mesh resolution will account for I_a and I_s, which control expansions in the far wake The mechanical turbulence, I_m, is caused by the turbine blade in the form of tip and hub vortices and the blade trailing edge wake which influence the rate of wake spreading in the near wake. This additional turbulence intensity is required when using a BEMT representation and was achieved by applying uniformly distributed turbulent kinetic energy source terms over the turbine disc. Burton *et al* (2001, Section 2.10) discusses possible empirically derived expressions for the likely additional turbulence within the wake. . Figure 5 compares the initial rate of growth of the near wake for additional turbulence intensity at the turbine of 0, 5 and 10 % with a rate of expansion by applying the method detailed in Burton *et al* (2001).

[insert Figure 5]

The near-wake growth estimate applies to a turbine operating in unbounded flow, whereas the domain used has a finite width and depth. The increased velocity in the bypass region increases the rate of far wake re-energisation which depend on I_s. The use of an I_m=5% turbulence

intensity compares reasonably well with the theoretical predictions for the early part of the wake, before the blockage effects have too great an impact, and is used for subsequent computations.

In an earlier phase of the work a coarse mesh was constructed using unstructured tetrahedral elements. The wake was seen to spread in a qualitatively correct manner. However, when a finer hexahedral mesh was used a much lower rate of wake spreading was found (I_m=0%). The seemingly correct initial behaviour for the coarse mesh is associated with the high values of numerical diffusion for a mesh of tetrahedral cells,

3. HATT Array Analysis

A 20m diameter HATT turbine operating in 40m water depth with turbine axis lateral spacing of 2D, 4D and 6D and a tip clearance of 10m are considered. Table 1 summarises the computational parameters applied in these simulations. The turbine is run at optimum TSR, $\lambda = 9.2$,for a fixed pitch and domain inflow speed of 2m/s.

[insert Table 1]

3.1 Mesh Generation

A structured hexahedral mesh was generated using ICEM, ANSYS(2006). The multi-block structure is presented in Figure 6 which shows the embedded cylinder zone for the turbine. An inlet boundary was placed 5D upstream, an outlet 10D downstream with a water depth 2D. No free surface effects were included. In order to simulate a realistic transverse array, the width of the domain was taken to be 2D, 4D, or 6D. The application of a slip boundary condition on the sidewalls simulates the performance of a turbine within a transverse array as any significant rotational flow is confined to the immediate vicinity of the wake.

[insert Figure 6]

In order to understand the influence of mesh density on the CFD solution a series of three meshes were built. An initial base mesh of approximately 1M elements was built for the 6D case. This mesh consisted of 40 nodes upstream of the turbine, 5 nodes axially along the turbine and 150 nodes downstream. The turbine disc was modelled using 76 nodes circumferentially and 36 radially from the edge of the hub. 10 nodes where placed above and below the turbine and 25 nodes laterally either side. The minimum cell face orthogonality angle was 51.9^{o}. maximum cell aspect ratio 159.3 and the maximum mesh expansion ratio was 5.4. Two, successively finer, meshes were generated by refining the edges in all directions using a mesh refinement factor of $\sqrt{2}$. The wake region 10D long consists of 396340 cells out of 1M for the coarse mesh which can be compared with O'Doherty *et al* (2009) who used 1M in close proximity to a pair of contra-rotating blades and 90000 cells elsewhere.

3.2 Boundary Conditions

A constant inflow condition of 2m/s was applied upstream. An outlet boundary condition of zero pressure gradient was applied downstream. The side walls and the seabed were modelled with a free slip wall. Although a volume of fraction approach can be used to capture the behaviour of the free surface, for the load condition of the turbine the analysis of Whelan *et al* (2007) was applied and showed the likely free surface deflections would be small (~0.05m) and thus a slip condition is applied. The use of a slip boundary conditions for the lateral boundaries represents the behaviour of the turbine within a transverse array of turbines. In practice, there will be a vertical shear profile at the inlet, a variable seabed bathymetry and a surface seastate inducing velocity

variations. In this study a uniform velocity inflow and a constant cross-section are applied as it is the influence on the wake evolution of I_m, mesh density and lateral spacing that are studied.

3.4 Computational Resources

Simulations were performed using the University of Southampton Iridis 2 Linux Cluster. The wall clock runtimes for the various meshes are given in Table 2. It can be noted that in these simulations the BEMT code requires a very small fraction of the overall computational resource. The computations made use of a parallel machine and provide a measure of the computational cost required. If the full turbine was modelled at a sufficient resolution to capture the blade generated wake and tip vortex it is likely that a much higher mesh density will be required in the near wake requiring at least one to two orders of extra computational power, Phillips *et al* (2009).

[insert Table 2]

4. RESULTS

4.1 Mesh Sensitivity

Example axial wake profiles are illustrated in Figure 7 for the 2D turbine seperation case for the coarse, medium and fine grids at spacings of 1D, 5D and 10D downstream of the turbine. Close to the turbine the difference in the velocity profile predicted by the coarse and fine mesh is small <4% of the maximum velocity deficit 1D downstream. Further downstream this difference has risen to 28%. The increased numerical diffusion on the coarser meshes leads to faster mixing of the wake region and consequently reduced velocity deficits downstream of the turbine. Achieving

a mesh independent solution for such a large wake region requires many millions of elements, however from this study it is considered that a fair approximation of the downstream wake can be achieved with the medium mesh of nearly six million elements of which 40% are within wake.

[insert Figure 7]

4.2 Influence of Swirl

The coupled RANS-BEMT approach allows the swirl induced by the passage of the turbine blades to be included in the simulation. Figure 8 compares the velocity profile downstream of the turbine for the 2D turbine seperation case. Including the swirl component slows the wake mixing process, such an effect is not present in the small scale experiments using porous discs or in computations that just apply a loss of axial momentum.

[insert figure 8]

4.3 Effect of Turbine Separation

The effect of turbine separation on the downstream wake is illustrated in Figure 9 which shows the wake profile for the 2D, 4D and 6D turbine separation cases. Blockage due to the presence of the turbine leads to acceleration of the flow either side of the turbine to maintain a constant mass flow rate. The smaller the turbine separation the more pronounced this effect becomes, Whelan *et al* (2009). This increased velocity results in larger velocity gradients which lead to more rapid mixing of the wake. Consequently the wake for the 2D separation case mixes faster than the 6D

separation case. The increase in velocity within the bypass region can be clearly identified and compares well with the average values from Whelan.

[insert Figure 9]

5. Prediction of Energy Capture for an Array of HATTs

In order to determine the power absorption of a tidal turbine placed downstream of the original turbine, velocity profiles where extracted from the RANS-BEMT simulation at distances of 1 to 9 diameters downstream in increments of 2 diameters, see Figure 10. The circumferential average axial velocity distribution was evaluated and used as an input into the BEMT code to determine the power output of an identical 20m diameter turbine in that location downstream. It was assumed that the turbine operates as a fixed pitch, constant RPM machine and thus when operating in the wake its performance will no longer give maximum Cp. The use of a constant diameter is associated with the need to operate in both directions of the tide. Although this analysis neglects the interaction of the downstream turbines on the flow, the BEMT coupling method could be applied by repeating the block structure at the appropriate distances downstream. It is also worth noting that Figure 10 illustrates the near wake region where the maximum velocity deficit is towards the turbine tip and this collapses into the typical far wake Gaussian distribution.

[insert Figure 10]

Figure 11 shows the normalised power expected at the five locations for the three different transverse spacings. The gradual recovery of energy within the wake is seen for greater distances downstream. The pitch and chord distributions of turbine blades could be optimised to operate in

such a wake to take account of the Gaussian distribution of the likely axial velocity deficit although the likely meanders of the wake, Larsen *et al* (2008), would reduce the deficit towards the hub.

[insert Figure 11]

As a preliminary estimate it has been assumed for multiple lines of turbines extending downstream that the power output from each successive line will be reduced by the same factor, consequently the total power P_T produced at a 1km^2 site normalised with respect to the upstream turbines performance, P_o will be:

$$\frac{P_T}{P_0} = N\left[1+\left(\frac{P}{P_0}\right)^1+\left(\frac{P}{P_0}\right)^2+.....+\left(\frac{P}{P_0}\right)^{n-2}+\left(\frac{P}{P_0}\right)^{n-1}\right] \quad (8)$$

where N is the lateral number of turbines per km, n is the number of longitudinal turbines (including the upstream turbine), and P/P_0 is the normalised power output for a downstream turbine for a given lateral and longitudinal spacing.

The total power (P_T/P_0) produced by a 1km^2 HATT array arranged in a rectilinear grid of varying longitudinal and lateral spacing's is presented in Table 3 and Figure 12. The highest total power potential is achieved with the smallest lateral spacing of 2D, while the optimum longitudinal spacing occurs at around 7D. Based on these results for a flow speed of 2m/s, with a free stream power absorption, $P_{0,}$ of 623.7kW, a total power extraction of 58.5MW could be achieved with 175 20m diameter turbines. This assumes that the inflow Q into the 1km wide, 40m deep channel is not strongly influenced by the blockage associated with all the turbines. However,

it should be noted that for this case the overall power coefficient for the 1km wide, 40m deep channel is 0.35 and depending on the local bathymetry there would be an impact on Q. If it can be assumed that the turbine array is within a channel where the flow speed is related to the head difference between exit and entrance then based on (1) the maximum power will occur for a Cp of 0.22. In this case 36MW is the maximum power that can be extracted. Examining Table 3 and Equation (8) indicates that this condition can be achieved with a lateral spacing of 2D and two rows of 25 turbines 9D apart, e.g. 50 turbines. For both the 4D and 6D spacings insufficient transverse rows can be used in a 1km distance to extract the maximum power from the site.

[insert Table 3]

[insert Figure 12]

The arrays considered so far are based on a rectilinear grid. However it has been noted that due to the blockage effect of other turbines placed laterally an accelerated region of flow is found outside the wake region. By using a staggered grid, Figure 13, this could be exploited to increase the power extraction potential of a site. Figure 14 shows predicted power output for offset downstream turbines. It can be observed that the offset turbines have an increased performance compared to free stream when positioned a short distance downstream.

[insert Figure 13]

[insert Figure 14]

6. Conclusions

An efficient method of capturing the wake downstream of a tidal energy convertor using a coupled blade element momentum approach embedded within a steady solution of the Reynolds Averaged Navier Stokes equations has been presented. Such an approach will allow the important influences of the seabed, the turbines own support structure, other tidal devices and the interaction with the free surface to be captured without the need to resolve the time accurate unsteady flow of a rotating turbine blade. This is achieved through use of a formulation that allows a straightforward iterative approach to fully couple the actual momentum changes (axial, tangential) to the lift and drag generated by each blade element from blade root to tip. The resultant approach is suitable for use in evaluating the energy capture of arrays of TEC at specific sites of know bathymetry with a significantly reduced computational cost

With regard to the RANS calculations for an isolated tidal energy convertor it has been shown that:

(i) Turbulent mixing of the wake is sensitive to the mechanical turbulence induced by the blades. In using techniques, such as BEMT, to provide the time averaged performance of a TEC it is essential that this influence is incorporated within the outer domain. This is achieved by adding suitable turbulent kinetic energy source terms in addition to the momentum sources.

(ii) Swirl induced in the flow by the turbine in generating power alter the rate of growth of the wake and this effect needs to be modelled

(iii) The wake growth is dependent on the mesh resolution used. In the case of a coarse mesh numerical diffusion effects determine the wake expansion. Mesh refinement studies are essential to identify the magnitude of such effects. Likewise, the design of a good quality mesh, adapted to the likely wake expansion is required to ensure that such effects are minimised. A high mesh resolution of at least 20 cells per D of axial distance is required to adequately capture the growth of a turbine wake.

Preliminary estimates of the power output for a 1km^2 MCT array have been performed for a variable number of turbines. These use the evaluation of the mean axial flow field at the likely longitudinal position of a row of turbines and include the influence of a column of turbines at a suitable lateral spacing. These show that power production is sensitive to both lateral and longitudinal separation relative to the mean tidal direction. It is seen that for bi-directional tidal flow a small lateral separation and large longitudinal separation is the most effective combination. For the assumed tidal flow of 2m/s with 20m diameter turbines in a 1km channel with water of 40m depth the optimum power capture of 36MW was achieved using two rows of 25 turbines. The longitudinal separation of the turbine rows can be reduced by staggering the rows.

Acknowledgements

This work is part of the on-going research into maritime energy within the School of Engineering Sciences (SES) through part-funded PhD studentships of Nicholls-Lee and Phillips.

References

ANSYS CFX/ICEM, 2006, User guide version 11.

Antheaume, S., Maıtre, T., Achard, J-L, 2008. Hydraulic Darrieus turbines efficiency for free fluid flow conditions versus power farms conditions, *Renewable Energy* 33, 2186–2198.

Bahaj, A.S., Molland, A.M., Chaplin, J.R., Batten, W.M.J. 2007a. Power and thrust measurements of marine current turbines under various hydrodynamic flow conditions in a cavitation tunnel and a towing tank, *Renewable Energy* 32, 407–426.

Bahaj, A.S., Myers, L.E., Thomson, M, Jorge, N. 2007b. Characterising the wake of horizontal axis marine current turbines, *Proceedings of the 7th European Wave and Tidal Energy Conference*, EWTEC 2007, 11-14 Sep., Porto, Portugal.

Barnsley, M.J., and Wellicome, J,F., 1993. Dynamic models of wind turbines – Aerodynamic model development. Final Report on Contract JOUR 0110 for the Commission of the European Communities Directorate-General XII Science, Research and Development

Barth, T.J., and Jesperson, D.C, 1989, The design and application of upwind schemes on unstructured meshes, AIAA Paper 89-0366.

Batten, W.M.J., Bahaj, A.S., Molland, A.F. and Chaplin, J.R. 2008. The prediction of the hydrodynamic performance of marine current turbines. Renewable Energy, 33, (5), 1085-1096.

Blanchfield, J., Rowe, A., Wild, P., and Garrett, C. 2007. The Power Potential of Tidal Streams including a Case Study for Masset Sound, *Proceedings of the 7th European Wave and Tidal Energy Conference*, EWTEC 2007, 11-14 Sep., Porto, Portugal.

Burton, T., Sharpe, D., Jenkins, N., and Bossanyi, E., 2001, Wind Energy Handbook, Wiley.

Garrett, C., and Cummins, P. 2005. The power potential of tidal currents in channels, *Philosophical Transactions of the Royal Society* A 461, 2563–2572.

Garrett, C., and Cummins, P. (2007). The efficiency of a turbine in a tidal channel, *Journal of Fluid Mechanics*, 588, 243–251.

Garrett, C., and Cummins, P. (2008). Limits to tidal current power, *Renewable Energy* 33, 2485–2490.

Grant, S., and Stallard, S., 2008. Modelling a Tidal Turbine in Unsteady Flow. In Proceedings of the eighteenth international offshore and polar conference, Vancouver, BC Canada, July 6-11, pp 473-479.

Hardisty, J., 2009, The analysis of tidal stream power. Wiley-Blackwell, Chichester, U.K.

Jarrin, N, Benhamadouche, S, Laurence, D and Prosser, R (2006). A synthetic-eddy-method for generating inflow conditions for large eddy simulations, *International Journal of Heat Fluid Flow*, 27, 585-593.

Jimenez, A, Crespo, A., Migoya, E. and Garcia, J., 2008, Large-eddy simulation of spectral coherence in a wind turbine wake, Environmental Research Letters, 3, 015004 (9pp) doi:10.1088/1748-9326/3/1/015004.

Jo, C-H, Park, K-K, and Im, S.W.(2007). Interaction of Multi Arrayed Current Power Generations *Proceedings of the 7th European Wave and Tidal Energy Conference*, EWTEC 2007, 11-14 Sep., Porto, Portugal

Larsen, G.C., Madsen, H.A., Thomsen, K. and Larsen, T.J., 2008, Wake Meandering: A Pragmatic Approach, Wind Energy 11:377–395

McCann, G.N. 2007. Tidal current turbine fatigue loading sensitivity to waves and turbulence – a parametric study, *Proceedings of the 7th European Wave and Tidal Energy Conference*, EWTEC 2007, 11-14 Sep., Porto, Portugal.

Myers, L., and Bahaj, A.S., 2007. Wake studies of a 1/30th scale horizontal axis marine current turbine. Ocean Engineering, Vol. 34, pp 758-762.

Myers, L.E., Bahaj, A.S., Rawlinson-Smith, R.I., and Thomson, M., 2008. The effect of boundary proximity upon the wake structure of horizontal axis marine current turbines, Proceedings of OMAE, Estoril, Portugal, 2008, OMAE2008-57667.

Nielsen, F.G., Argyriadis, K., Fonseca, N., Le Boulluec, M., Liu, P., Suzuki, H., Sirkar, J., Tarp-Johansen, N.J., Turnock, S.R., Waegter, J. and Zong, Z., 2009, [Report of] Specialist Committee V.4: ocean, wind and wave energy utilization. Proceedings of the 17th International Ship and Offshore Structures Congress. Seoul National University, Korea, 201-257.

O'Doherty DM, Mason-Jones A, O'Doherty T, and Byrne CB, 2009, Considerations of improved tidal stream turbine performance using double rows of contra-rotating blades, Proc. of 8th European Wave and Tidal Energy Conference, Uppsala, Sweden.

Phillips, A.B., Turnock, S.R., and Furlong, M.E., 2009, Evaluation of manoeuvring coefficients of a self-propelled ship using a Blade Element Momentum propeller model coupled to a Reynolds averaged Navier Stokes flow solver, Ocean Engineering, 36, 1217-1225.

Phillips, A.B., Turnock, S.R. and Furlong, M.E. (2010) Accurate capture of rudder-propeller interaction using a coupled blade element momentum-RANS approach. Ship Technology Research (Schiffstechnik), 57, (2), 128-139.

Sinha, M, Katz, J, and Meneveau, C, 2000, Quantitative visualisation of the flow in a centrifugal pump with diffuser vanes –II: addressing passage-averaged and Large Eddy Simulation modelling issues in turbomachinery flows, J. Fluids Engineering, 122, 108-116.

Sørensen, J.N., and Shen, W.Z., 2002, Numerical Modeling of Wind Turbine Wakes, Journal of Fluids Engineering, Vol. 124, 393-399

Sun, X., Chick, J.P.,and Bryden, I.G., 2008. Laboratory-scale simulation of energy extraction from tidal currents. Renewable Energy, Vol. 33, pp 1267-1274.

Turnock, S.R., Pashias, C. and Rogers, E., 2006, Flow feature identification for capture of propeller tip vortex evolution. Proc. of the 26th Symposium on Naval Hydrodynamics. Rome, Italy, 223-240.

Turnock, S.R., 2006, Predictions of hydrodynamic performance of horizontal axis tidal turbines, Report 1878, Wolfson Unit for Marine Technology and Industrial Aerodynamics.

Turnock, S.R., Phillips, A.B. and Furlong, M. (2008) URANS simulations of static drift and dynamic manoeuvres of the KVLCC2 tanker. In, SIMMAN 2008: workshop on verification and validation of ship manoeuvring Simulation Methods, Lyngby, Denmark, 13-17 April.

Whelan, J.I., Graham, J.M.R., and Peiro, J, 2009, A free-surface and blockage correction for tidal turbines, J. Fluid Mech, vol 624, pp281-291.

List of Tables

Table 1 Computational parameters used for the CFD simulations

Parameter	Setting
Simulation Type	Steady State
Computing	n times 64 bit 2.2GHz processors with 2Gb of RAM each asl part of the University of Southampton Iridis 2 Computer Facility
Mesh Type	Block structured hexahedral
Turbulence Model	k-ε model
Advection Scheme	CFX High Resolution
Convergence Control	RMS residual $<10^{-5}$

Table 2 Computing Resource Requirements

Mesh	No. of Elements	No. of Processors n	Memory (GB)	Runtime
Base 6D	1,094,288	1	4	11hrs 14min
Medium 6D	3,261,531	6	6	6hrs 20min
Fine 6D	9,576,315	20	10	13hrs 47min

Table 3 – Normalised power potential of a 1km^2 site for different array spacing configurations.

		6D Lateral Spacing			4D Lateral Spacing			2D Lateral Spacing		
Long. Spacing		N = 8			N = 12			N = 25		
Diameters	N	P/P0	PT/P0	No. of Turbines	P/P0	PT/P0	No. of Turbines	P/P0	PT/P0	No. of Turbines
1	50.0	0.33	12.02	400	0.36	18.73	600	0.45	45.26	1250
3	16.0	0.49	15.53	128	0.52	24.93	192	0.63	66.28	400
5	10.0	0.58	18.93	80	0.59	29.06	120	0.72	85.80	250
7	7.0	0.64	21.44	56	0.68	34.82	84	0.78	94.10	175
9	5.0	0.71	22.40	40	0.73	35.47	60	0.82	87.39	125

List of Figures

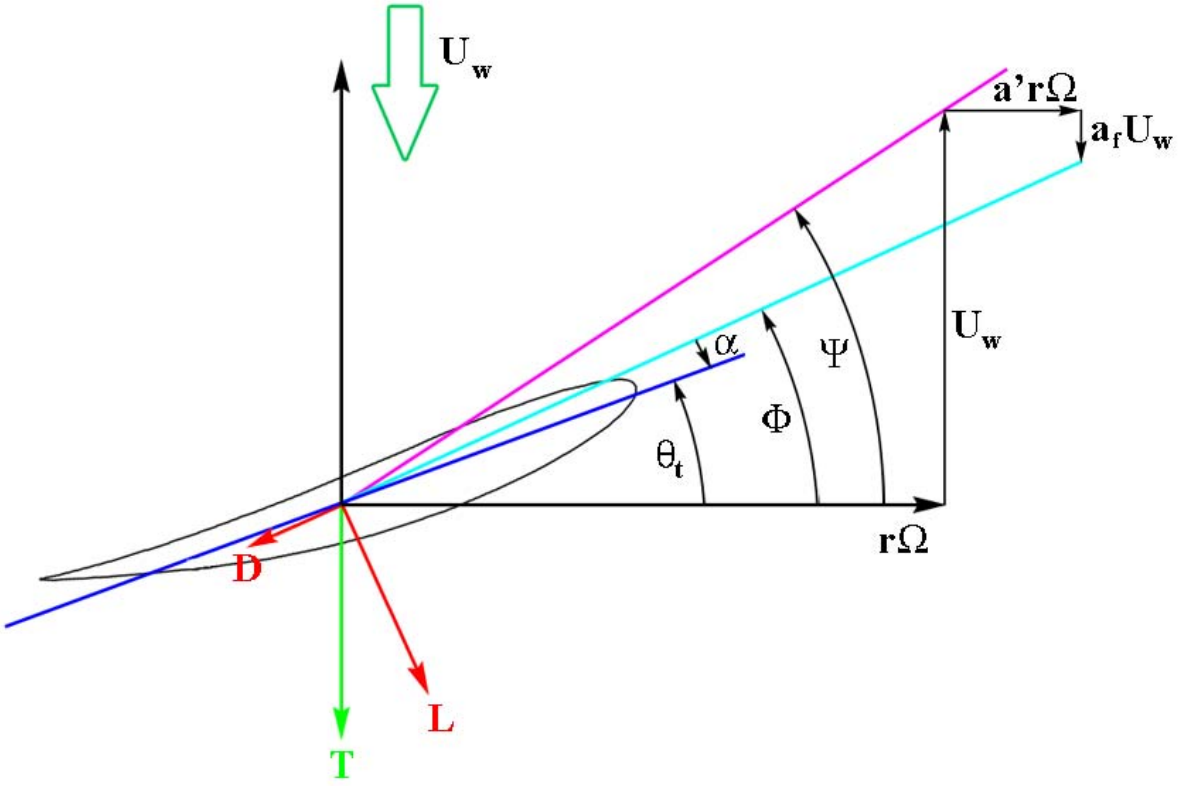

Figure 1 - Blade element velocity/force for a turbine section rotating at Ω at radius r operating in a wake velocity $U_w=w_f U_o$ where θ_t is the section design pitch angle.

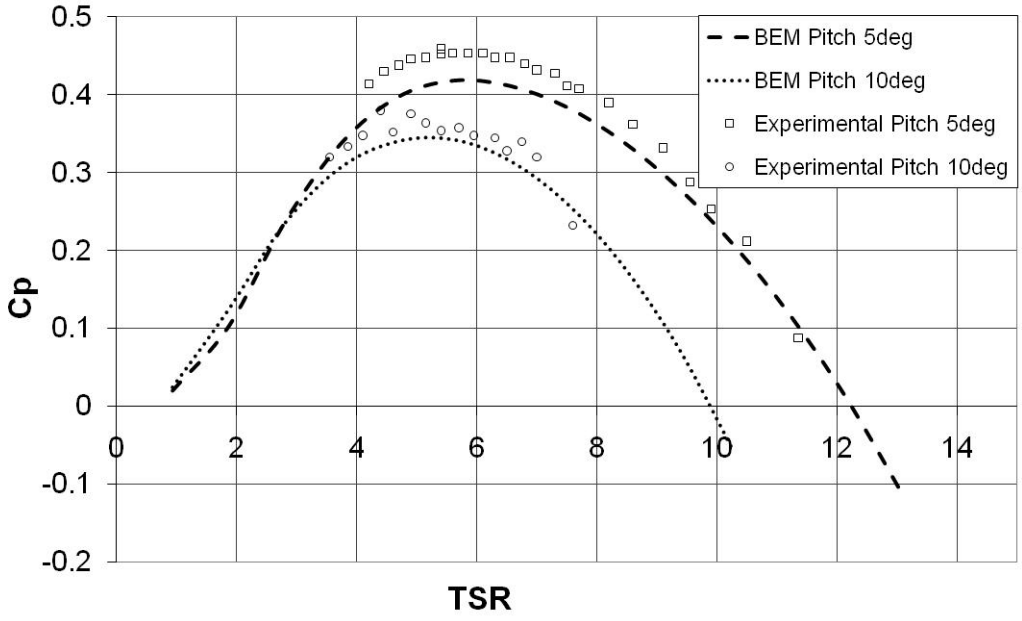

Figure 2 – Comparison of BEMT results and experimental data from Bahaj *et al* (2007) for power coefficient Cp varying with Tip Speed Ratio for two different blade root pitch angles.

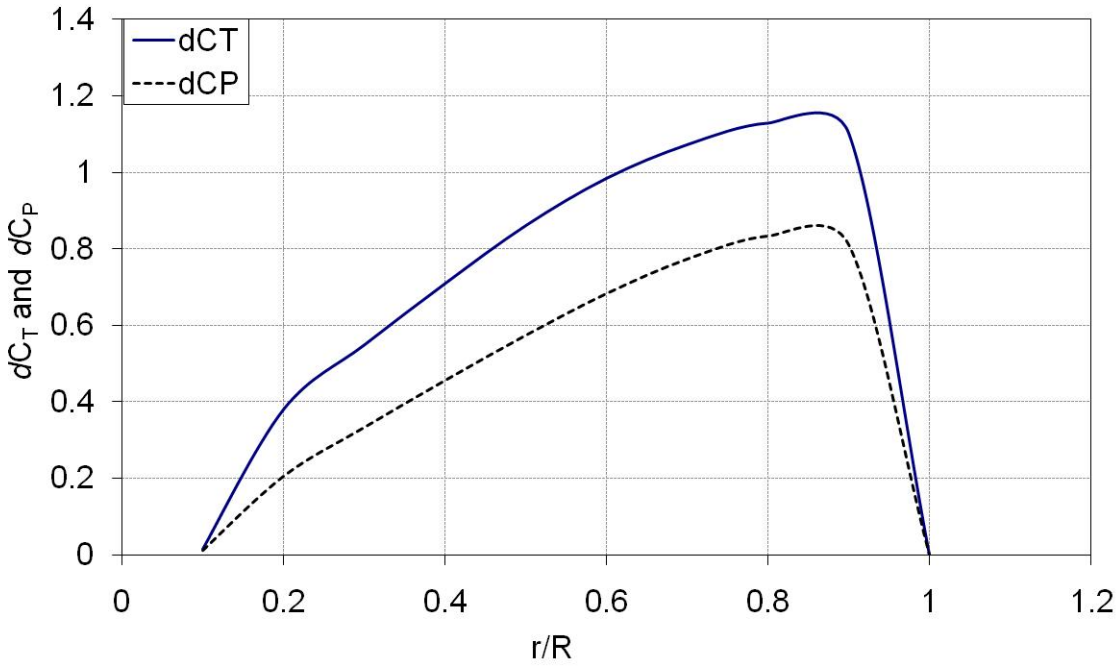

Figure 3 – Radial variation of elemental Thrust and Power coefficients for the three bladed turbine operating at optimum TSR of 9.2 and hub diameter ratio of 10%.

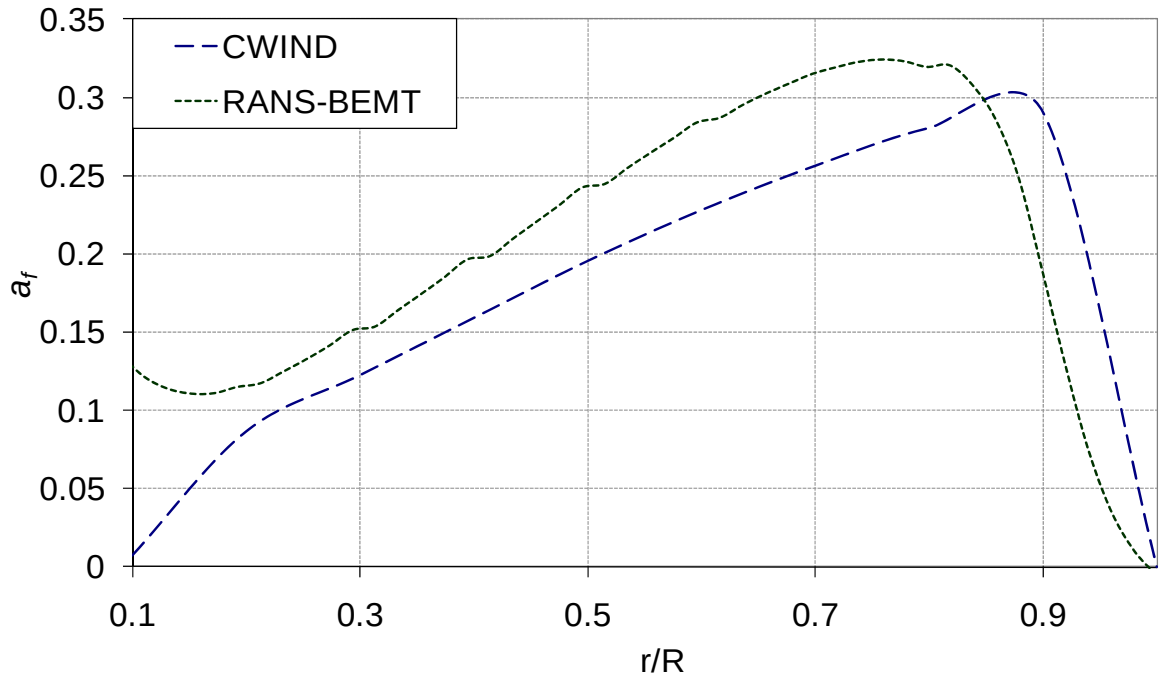

Figure 4 – Comparison of axial flow factors, a_f, evaluated initially by the BEMT code and those realised in the RANS-BEMT simulation.

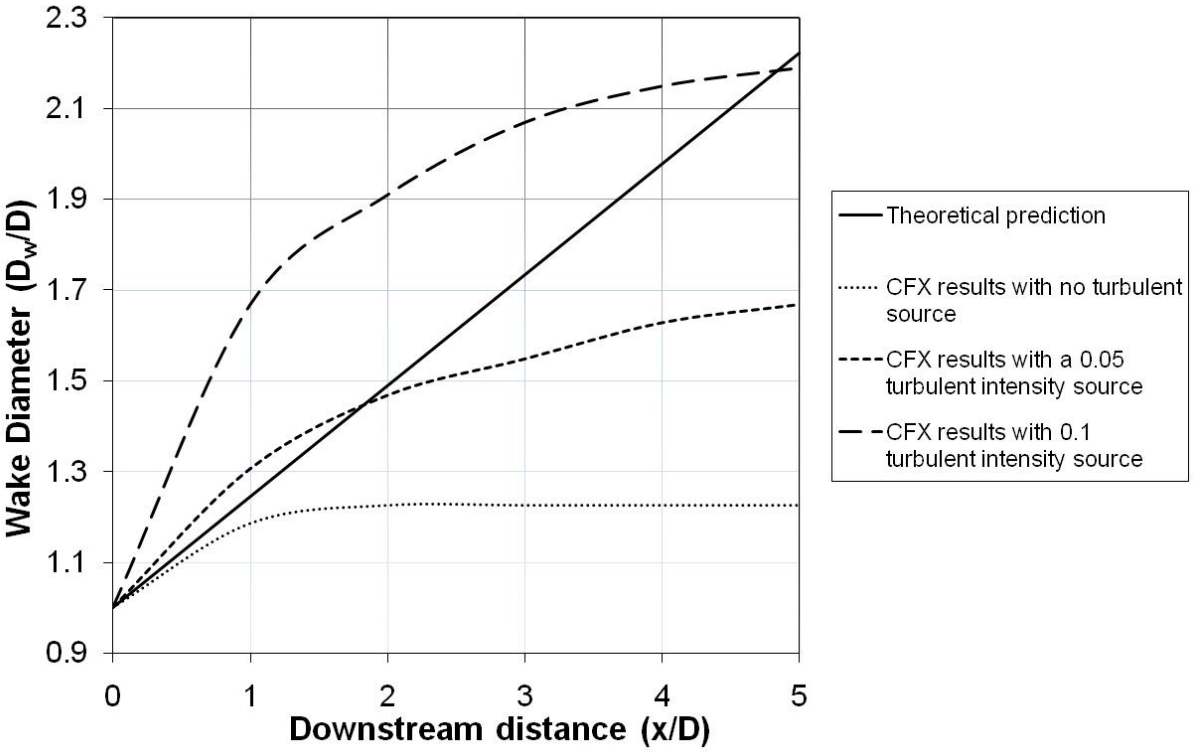

Figure 5 – Comparison of wake growth rate from theoretical prediction and CFD simulations with varying turbulence intensities at turbine location (Domain Width =6D)

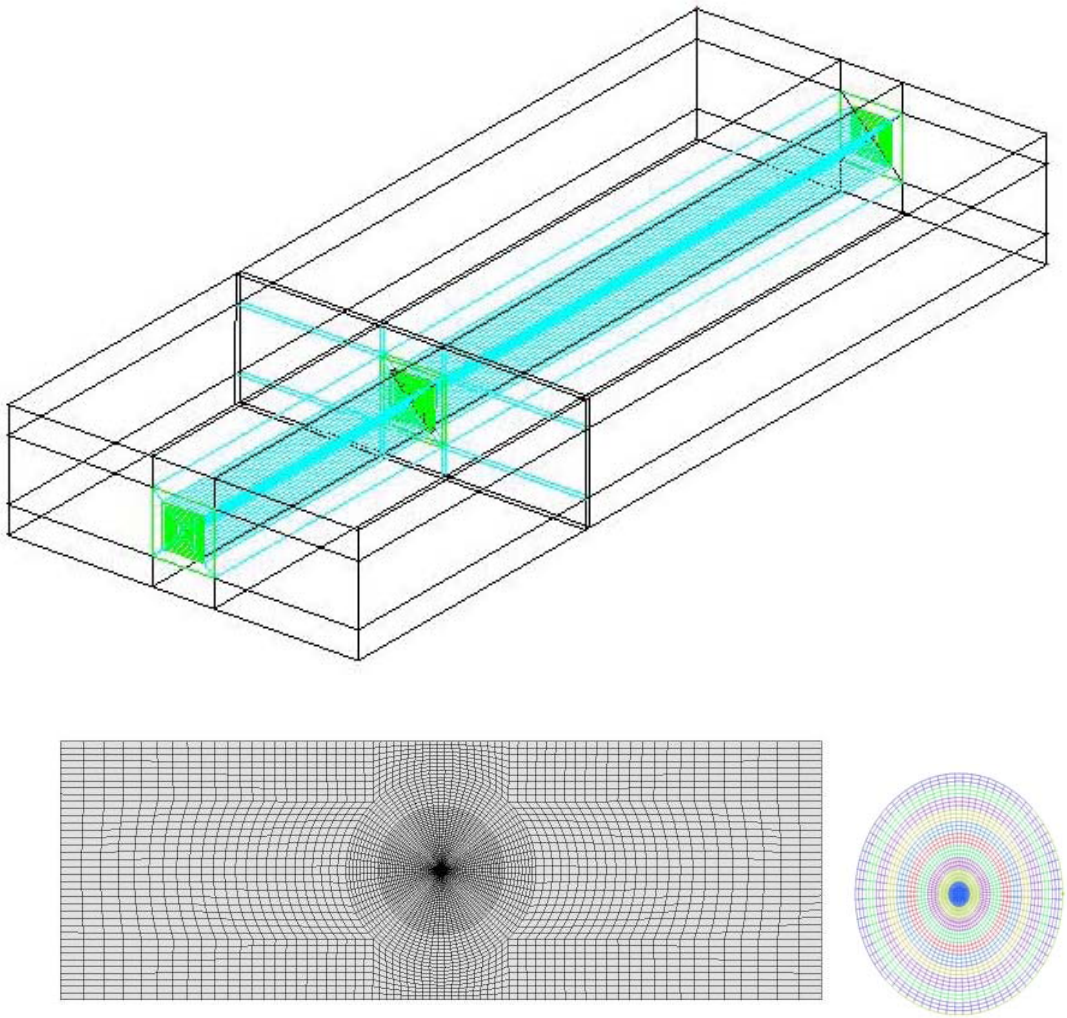

Figure 6 – Coarse Structured Mesh Blocking Structure, for 6D case *(top)*, end elevation of turbine mesh *(right)*and whole crosssection(*left*)

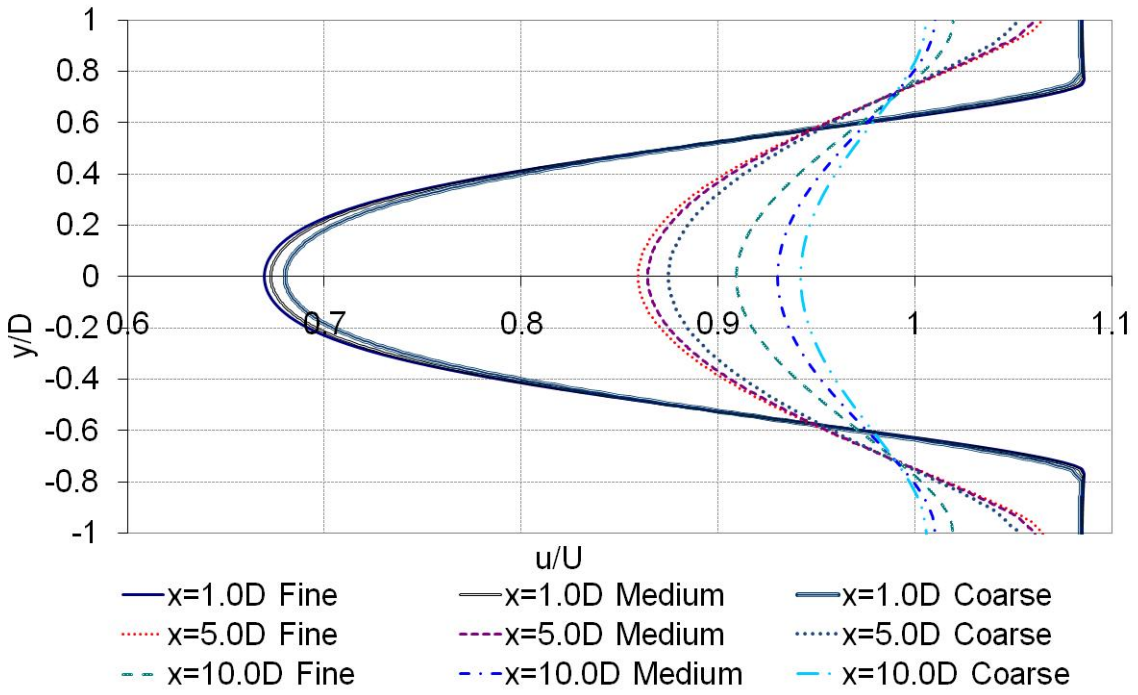

Figure 7 – Influence of Mesh Density on Downstream Wake Deficit for three levels of mesh refinement and three downstream locations.

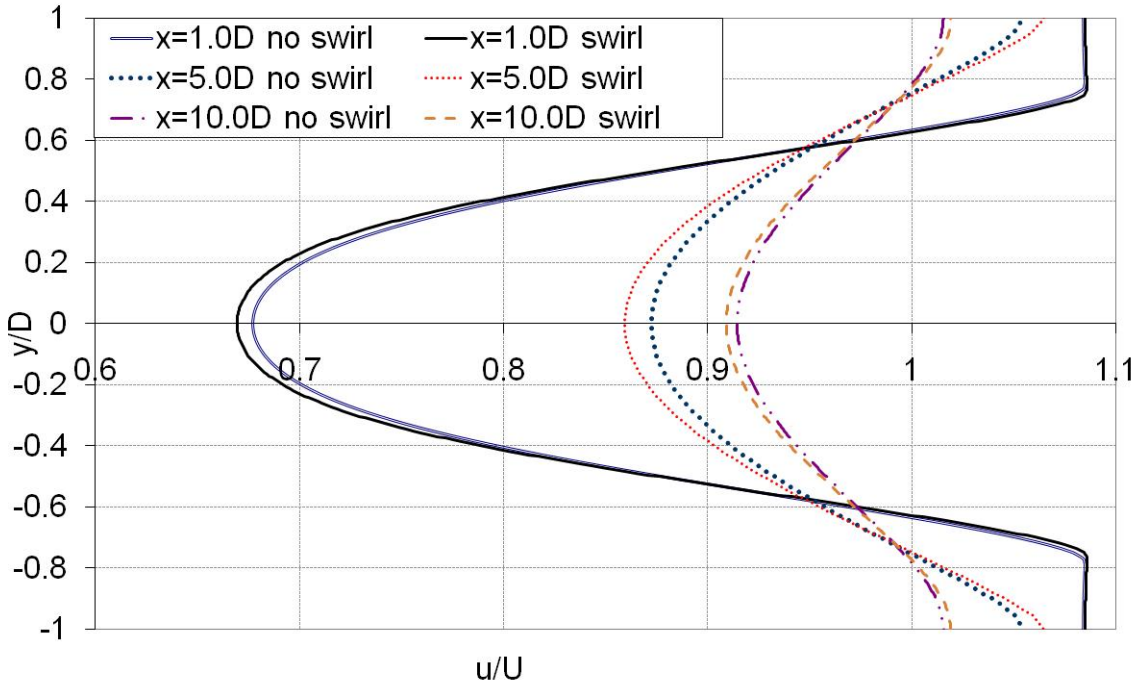

Figure 8 – Influence of Swirl on Downstream Wake Profile for medium mesh

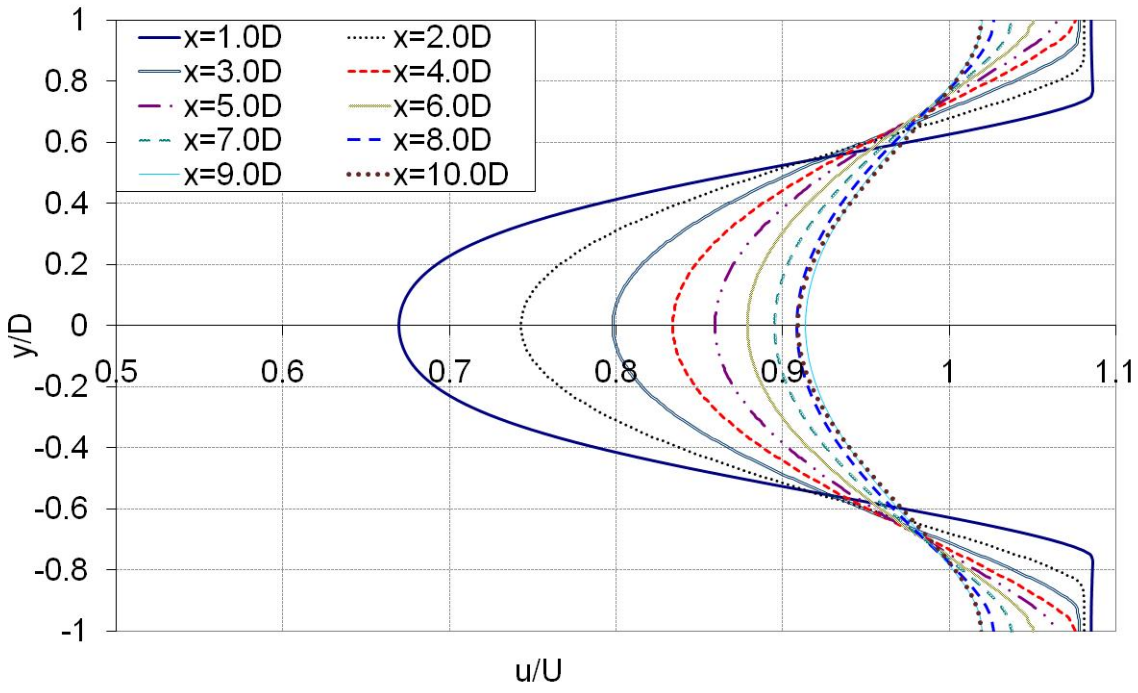
x=1.0D
x=2.0D
x=3.0D
x=4.0D
x=5.0D
x=6.0D
x=7.0D
x=8.0D
x=9.0D
x=10.0D
y/D
u/U
1
0.8
0.6
0.4
0.2
0
-0.2
-0.4
-0.6
-0.8
-1
0.5
0.6
0.7
0.8
0.9
1
1.1

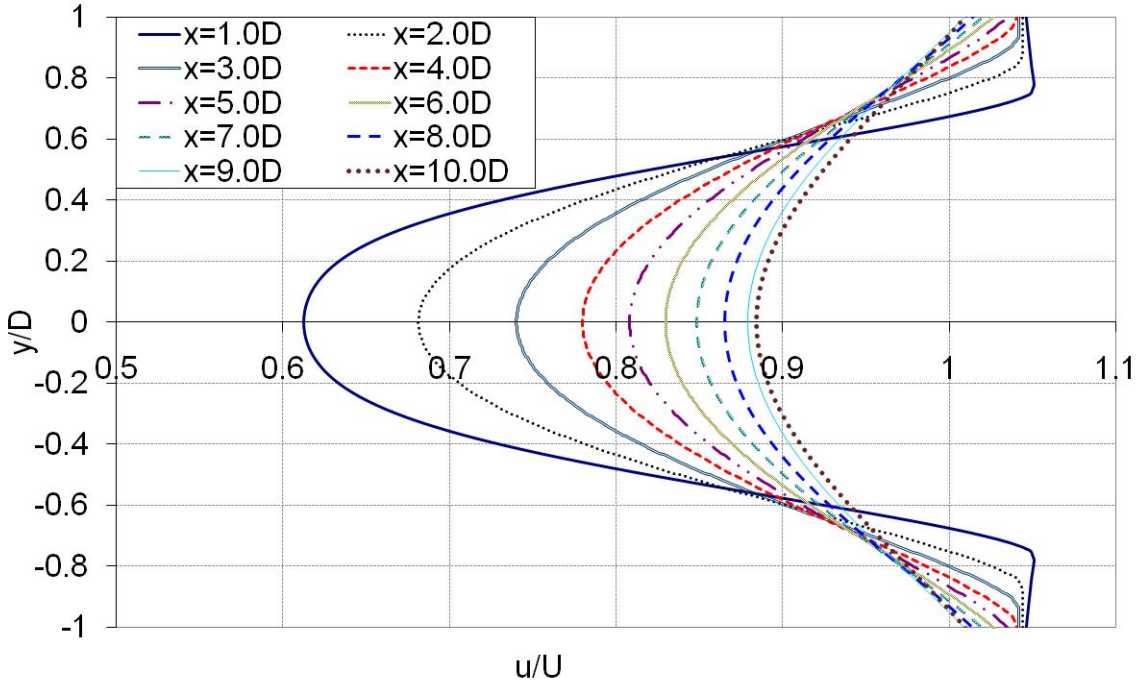
x=1.0D
x=2.0D
x=3.0D
x=4.0D
x=5.0D
x=6.0D
x=7.0D
x=8.0D
x=9.0D
x=10.0D
y/D
u/U
1
0.8
0.6
0.4
0.2
0
-0.2
-0.4
-0.6
-0.8
-1
0.5
0.6
0.7
0.8
0.9
1
1.1

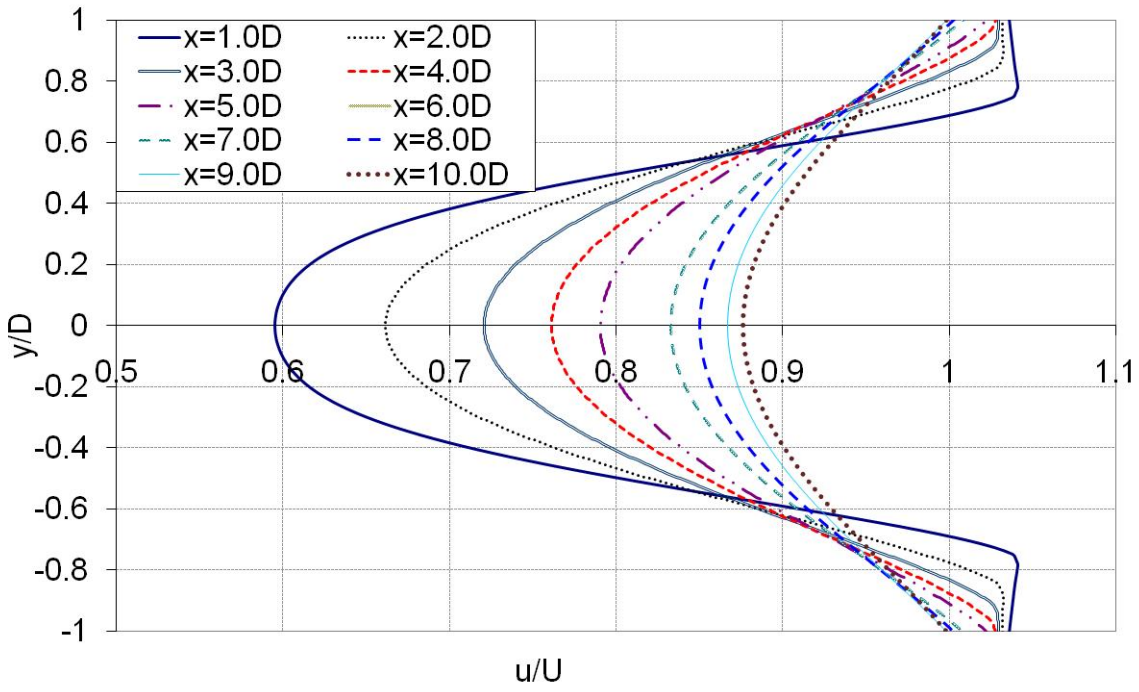

Figure 9 – Influence on lateral separation on downstream wake structure – lateral turbine separation = 2D *(top)*, lateral turbine separation = 4D *(middle)*, lateral turbine separation = 6D *(bottom)*

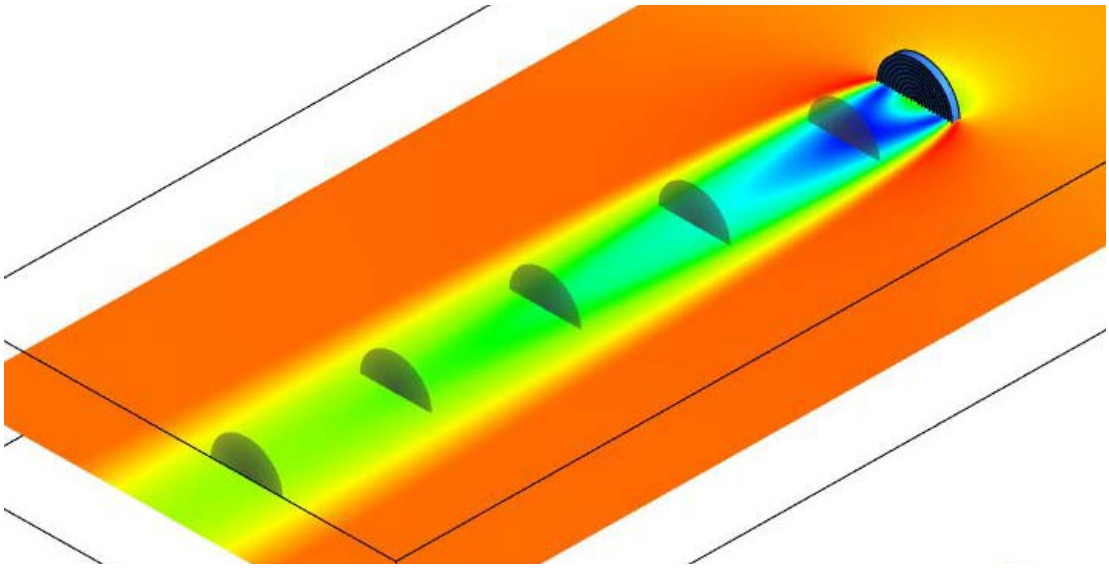

Figure 10 – Locations of average radial velocity extraction. Lateral turbine separation=6D. Blue represents slowest and Red fastest velocity.

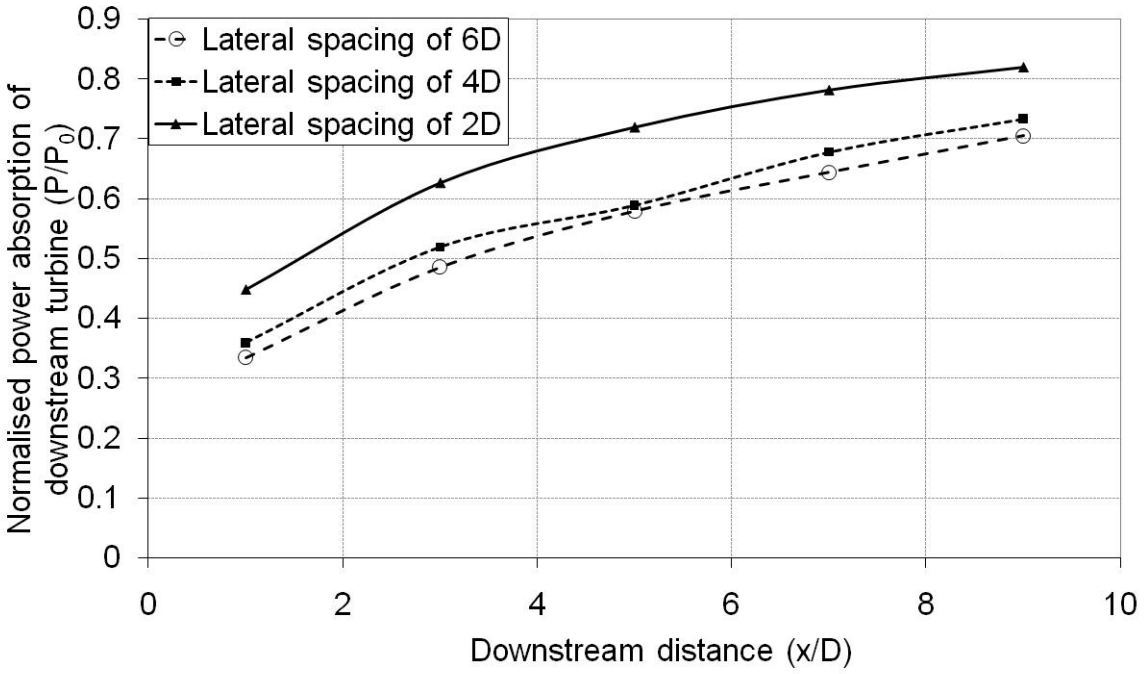

Figure 11 – Power absorption of a downstream turbine for varying lateral and longitudinal spacings

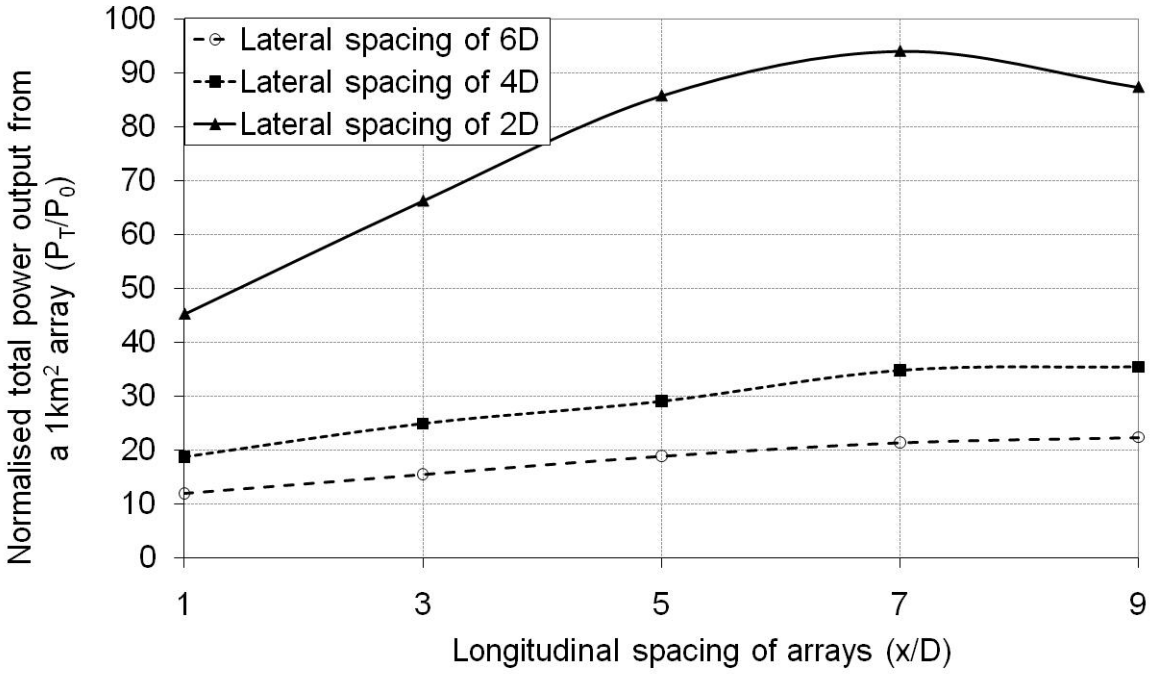

Figure 12 – Total power potential from a 1km square rectilinear array of MCT turbines with varying spacing configurations

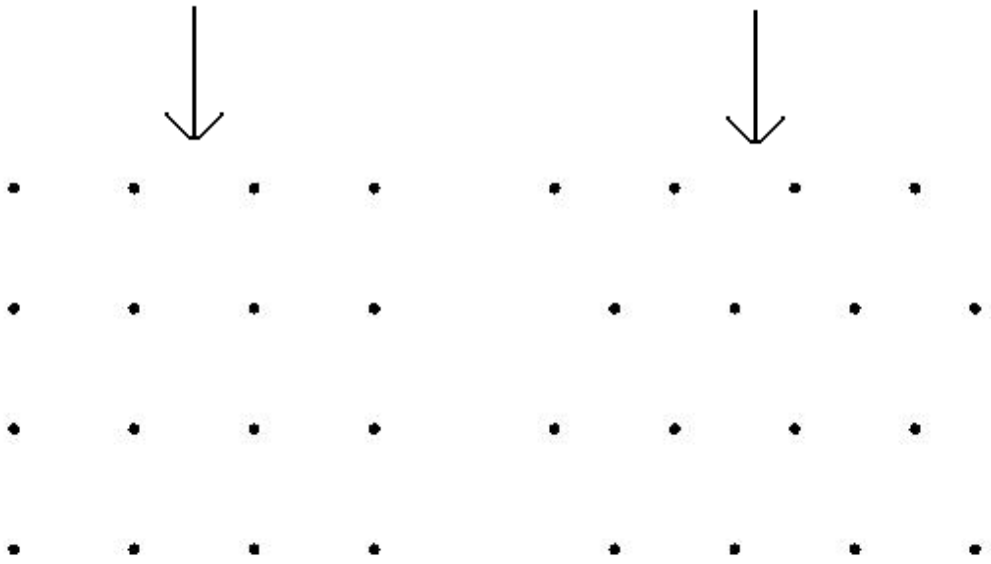

Figure 13 – Rectilinear Grid Array *(left)* and Staggered Grid Array *(right)*

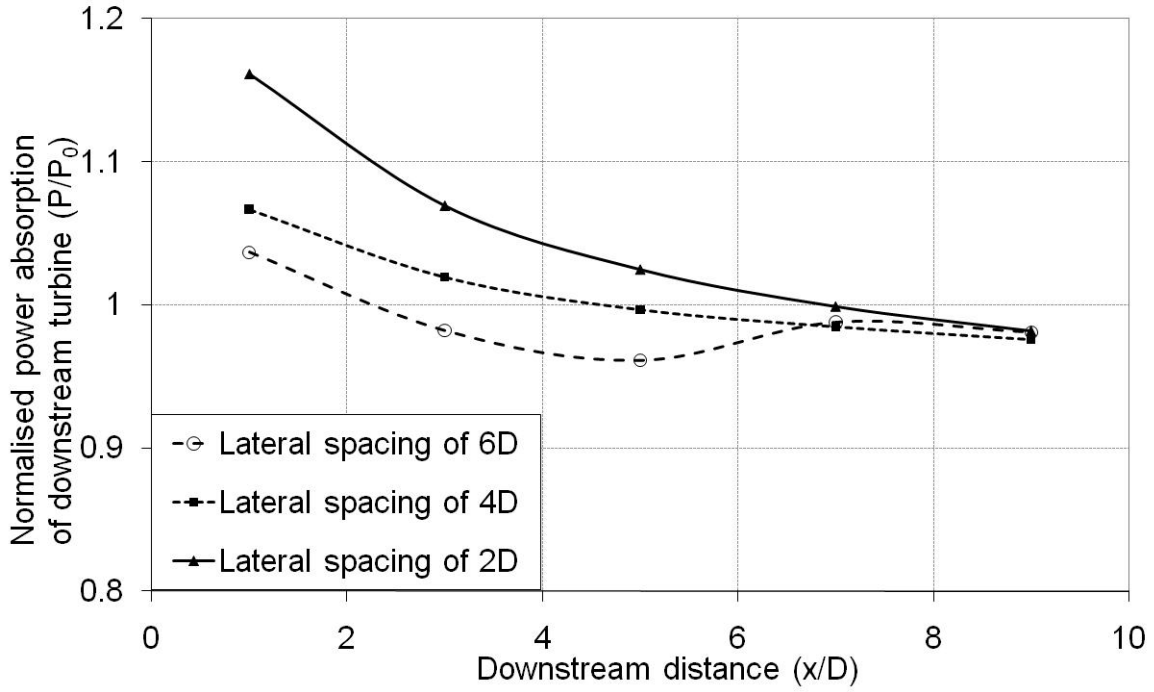

Figure 14 – Power absorption of an offset downstream turbine for varying lateral and longitudinal spacing